Title
Optimization of metal-supported solid oxide electrolysis cells with infiltrated catalysts

Journal
International Journal of Hydrogen Energy, 48(57)

ISSN
0360-3199

Authors
Welander, Martha M
Hu, Boxun
Tucker, Michael C

Publication Date
2023-07-01

DOI
10.1016/j.ijhydene.2023.03.039

Peer reviewed

Optimization of metal-supported solid oxide electrolysis cells with infiltrated catalysts

Martha M. Welander, Boxun Hu, and Michael C. Tucker*

Abstract:

Metal-supported solid oxide electrolysis cells (MS-SOECs) are being developed for steam-to-hydrogen electrolysis, especially for utilization of dynamic or intermittent electrical power from renewable sources. Various aspects of the electrocatalyst processing and composition, and metal support structure were explored. Catalyst materials, infiltration temperature and infiltration cycles were optimized for high performance and durability. Numerous catalyst materials were screened for both oxygen and steam electrodes. The oxygen catalyst had moderate impact on both initial cell performance and durability. Reducing Ni content in the steam electrode had little effect on durability, but reduced initial performance. Ex-situ XRD analysis and cell assessment of catalyst infiltration temperature revealed that the optimal range is 750 to 850 °C. The best cell performance and durability was achieved with LSCF-SDC oxygen electrocatalyst and SDC-Ni (60:40 vol%) steam electrocatalyst infiltrated 11 times at 800 °C and operated at 700 °C. At low steam content, a significant mass transport limitation on the steam side results in limiting current behavior. Thinner and more porous metal supports were implemented, and found to improve steam mass transport at low steam content, relevant for SOECs operating under high H_2 recycle rate or high steam utilization.

MS-SOEC; infiltration; optimization

*mctucker@lbl.gov

Phone 1-510-486-5304

Fax 1-510-486-4260

LBNL; 1 Cyclotron Rd; MS 62-203; Berkely CA 94720; USA

Introduction

Hydrogen offers a solution to decarbonize industrial processes and economic sectors where reducing emissions is both urgent and difficult. Hydrogen production is dominated by fossil fuel reforming, partial methane oxidation and coal gasification with poor environmental credentials[1]–[3]. Steam electrolysis allows for hydrogen production with reduced emissions and carbon neutrality provided that the electricity used is generated via renewable sources. Compared to low temperature electrolysis cells, solid oxide electrolysis cells (SOECs) boast higher hydrogen production rates for a given overpotential with lower electrical energy requirements, and do not require expensive precious metal catalysts[4], [5].

Conventional SOECs consist of two porous electrodes, the anode and the cathode, separated by an ionically conducting electrolyte. H_2O and/or CO_2 is electrochemically reduced at the cathode to produce H_2 and/or CO fuels and oxygen ions. Oxide ions are conducted through the dense electrolyte to the anode where they are oxidized to produce pure oxygen. High operating temperatures required for adequate SOEC performance (typically $\geq$ 700 °C) introduce thermal expansion, and allow for rapid formation of NiO in the cathode if it is exposed to oxidizing conditions. These changes make mechanical stress within the cell inevitable and comprise critical hurdles that must be overcome for successful SOEC commercialization. For example, conventional SOEC sensitivity to redox and thermal cycling due to brittle ceramic components pose challenges to intermittent operation with renewable sources[6], [7].

Metal-supported SOECs (MS-SOECs) with porous stainless steel substrates may offer several advantages over conventional SOECs for intermittent operation when utilizing variable energy sources such as solar and wind. These advantages include low cost structural materials, mechanical ruggedness, and excellent tolerance to thermal and redox cycling (based on demonstrations in fuel cell mode). Operation of metal-supported cells in fuel cell mode (MS-SOFCs) is extensively studied, but limited work has been devoted to MS-SOECs. Like standard SOECs, MS-SOECs are often designed with reversible SOFC operation in mind but current development lags conventional SOECs [8]. Current MS-SOEC performance is typically below 0.8 A cm^{-2} at 1.3 V compared to >1 A cm^{-2} in standard SOECs [9]–[13]. To realize their

full potential, tailored optimization of MS-SOECs is necessary. Previously, our group has selected electrocatalysts for infiltration into MS-SOECs, identified Cr migration in the anode and catalyst coarsening in the cathode as primary degradation modes, and demonstrated the use of coatings on the stainless steel to reduce Cr migration[14]–[16]. This work further explores a number of material composition, processing, and operational parameters that influence MS-SOEC performance and durability. Symmetric-structured MS-SOECs with porous metal supports on both sides are utilized. This structure allows rapid catalyst infiltration and easy modification of the catalyst compositions, enabling numerous steam and aoxygen side electrocatalysts to be screened here. The processing temperature of the oxygen side electrocatalysts was investigated to determine sensitivity of crystalline phases and balance the risks of metal support oxidation and catalyst interdiffusion. Additionally, the catalyst loading and cell operating temperature are explored. The impact of these parameters on performance and durability is discussed. Finally, the impact of the metal support structure on mass transport limitation at low steam content is assessed.

Materials and methods

MS-SOECs consisting of thin ceramic scandia-ceria-stabilized zirconia (ScSZ) electrolytes, ScSZ scaffold backbone layers with infiltrated catalysts, and ferritic stainless steel supports were used for this work and prepared with techniques reported previously [17]. Detailed information on the MS-SOEC structure can be found in reference [8, 18], and a cross-section image of the cell structure is shown below in Figure 6. Standard cells were ~26 mm in diameter with 12 μm thick electrolyte, 25 μm thick electrodes, and 250 μm thick porous metal supports. Standard cell structure was used throughout this work, except where noted. The standard structure is the same as our group has used for several years, as reported in the references above. For comparison to standard cells, thinner and more porous metal supports were prepared by adding 50% additional poreformer (PMMA, Sekisui), and casting with a smaller gap between the

substrate and blade. Laminated green tapes were laser cut (Hobby model, Full Spectrum Laser) into button cells that were de-binded in air at 525 °C for 1h and sintered at 1350 °C for 2 h in 2 % H_2 in Ar, and pre-oxidized in air at 850 °C for 10 h to form a Cr-protective scale in the metal support [19], [20]. Air-side metal supports were coated with $CuMn_{1.8}O_4$ using electrophoretic deposition and heat treated at 1000 °C for 4 h in 2 % H_2 in Ar and at 750 °C for 5 h in air[14].

Cells were infiltrated by masking the edges with acrylic paint (Liquitex) and infiltrating with metal nitrate catalyst precursor solutions under vacuum. Catalyst solutions were prepared by mixing stoichiometric amounts of metal nitrates with Triton-X 100 (both Sigma Aldrich) in water to a total metal nitrate concentration of 3.3 M and 3.7 M for the cathode and anode, respectively. The entire pore volume of the electrode and metal support layers were filled with solution during each infiltration cycle, by using mild vacuum to extract air. The oxygen electrocatalyst was a composite of $La_{0.6}Sr_{0.4}Co_{0.2}Fe_{0.8}O_3$ and $Sm_{0.02}Ce_{0.8}O_{2-\delta}$ (LSCF – SDC) and the steam electrocatalyst was 40 vol% Ni-60vol% $Sm_{0.02}Ce_{0.8}O_{2-\delta}$ (SDCN40), except where noted. Oxygen and steam catalysts were infiltrated 11 times each and fired at 800 °C in air and calcined for 30 min between infiltrations to convert the precursors into the appropriate oxide phases, except as otherwise specified. In other studies, the oxygen electrocatalyst or steam electrocatalyst were varied, independently. Alternative oxygen catalysts tested were Pr_2NiO_4-SDC, La_2NiO_4-SDC, and LSCF- $Pr_{0.02}Ce_{0.8}O_{2-\delta}$ (PDC). Alternative steam catalysts tested were pure SDC, SDCN10, and SDCN60, with 0, 10, or 60 vol% Ni respectively.

Cell testing followed a published protocol[17]. Platinum wires and mesh were spot welded onto the electrodes for electrical connection. Cells were sealed onto 410 stainless steel rigs using glass paste (80 wt% glass powder, GM31107 Schott and 20 wt% ink vehicle, Fuel Cell Materials). Test rigs were placed inside tube furnaces and heated to 90 °C at 10° C/min, 200 °C at 2°C/min, and to 700 °C at 10 °C/min. Oxygen electrodes were exposed to static air and steam electrodes were flushed with N_2 followed by initial reduction in humidified H_2 (3% H_2O). Cells were considered fully reduced when the open circuit voltage (OCV) stabilized at ~1.10 V. Catalyst pre-coarsening was performed at 750 °C for 4 h prior to initiating

testing at 700 °C (or other operating temperature). The heated water bubbler and heat-traced lines delivering H_2 were heated to produce a 50/50% H_2O/H_2 mixture for electrolysis operation.

Electrochemical measurements were performed with a VMP3 multi-channel potentiostat and current booster (Biologic). Linear sweep voltammetry (LSV) recorded the I-V polarization curve with a sweep rate of 10 mV/s between the open-circuit voltage (OCV) and 1.4 V (vs. Ref). Electrochemical impedance spectroscopy (EIS) measurements were collected at OCV with an AC voltage amplitude of 5 mV over a frequency range of 100 mHz to 200 kHz. For durability testing, a constant current of 0.5 A cm^{-2} was applied.

XRD spectra were collected for LSCF powders fired between 650 and 950 °C to determine differences in phase and purity. LSCF powder was prepared by heating the catalyst precursor solution to 300 °C followed by 30 min firing at the desired temperature. Spectra were collected using a Bruker XRD between 20° and 80° 2θ at ambient temperature.

Results and Discussion

Oxygen Electrode

A variety of MS-SOEC oxygen electrocatalysts were screened for initial performance and durability. Catalyst selections were made based on previous work and literature studies. Conventional SOEC oxygen electrodes have often been composed of LSM or LSCF. While LSM is a good catalyst in the 800 to 900 °C range, LSCF has better performance at lower temperatures and was therefore selected as the baseline catalyst here for operation in the 650 to 750 °C range [21]. Addition of an ionic conductor into the oxygen electrode to form a composite catalyst significantly improves performance of MS-SOECs by expanding triple phase boundary lengths and increasing ionic conductivity[22]. Sm-doped ceria was used as the ionic conductor in our previous MS-SOEC work,[15] and is compared to Pr-doped ceria here. In conventional SOECs Pr-based materials provide faster oxygen incorporation that traditional perovskites such as LSC and LSCF, increasing performance [23]. Other promising oxygen electrocatalysts include

Ruddlesden-Popper phases due to their MIEC properties and good chemical stability [24]. Nickelates have recently received much attention due to their ability to accommodate larger over-stoichiometry of oxygen at the electrode-electrolyte interface better than other oxygen conducting materials[21], [25]. For these reasons, Pr_2NiO_4 and La_2NiO_4 were selected to represent these classes of catalysts.

Despite slight differences in initial performance, short term durability was similar for all oxygen electrocatalysts, Figure 1. Cells with LSCF-SDC and Pr_2NiO_4-SDC composite catalysts showed high initial performance with current density of 0.8 A cm^{-2} at 1.4 V. The performance of LSCF-PrDC was 0.68 A cm^{-2} at 1.4 V. Lowest performance was observed for the La_2NiO_4 SDC at 0.5 A cm^{-2} at 1.4 V. Based on short term durability, degradation rates are estimated to be ~20 % kh^{-1} for all catalysts after the first ~25 h of initial transients are complete. The similar degradation for all compositions implies that evolution of the oxygen electrocatalyst does not dominate degradation. This is consistent with recent post-mortem analysis of MS-SOECs after 1000 h operation, which ascribed degradation to steam electrode catalyst coarsening, Cr poisoning of the oxygen electrode, and oxidation of the metal support [16]. Based on these results, LSCF-SDC was selected for further optimization of the catalyst loading and infiltration processing temperature.

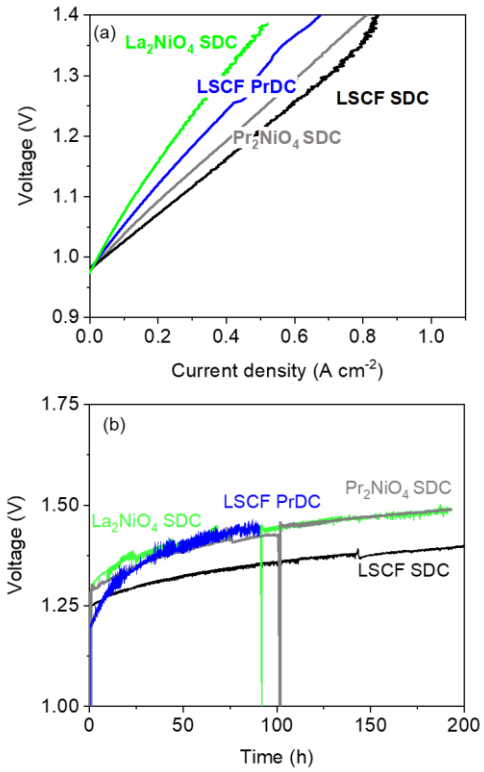

Figure 1. Oxygen electrode catalysts. (a) Initial performance and (b) durability of various oxygen electrodes for MS-SOECs at 700 °C and 50:50 H_2:H_2O. Steam electrodes are SDCN40 for all cells.

The infiltrated oxygen catalyst loading affects performance and durability. Cells were infiltrated with 7, 11 and 15 cycles of LSCF-SDC catalyst, Figure 2. Cells infiltrated 11 and 15 times displayed similar performance and durability. In contrast, 7 cycles of infiltration led to decreased performance and poor initial durability, likely due to inadequate catalyst loading to achieve good ionic and electronic percolation. EIS indicated larger polarization resistance compared to cells with more infiltration cycles, Figure 2b. This is consistent with previous reports that a threshold infiltration loading must be attained for good performance[26], [27]. It is expected that exceeding 15 cycles would over-fill the electrode and support pores, thereby decreasing performance due to mass transport limitation. Based on the similar results for 11 and 15 cycles, and the desire for fewer cycles to save fabrication time, 11 cycles was selected for all further optimizations.

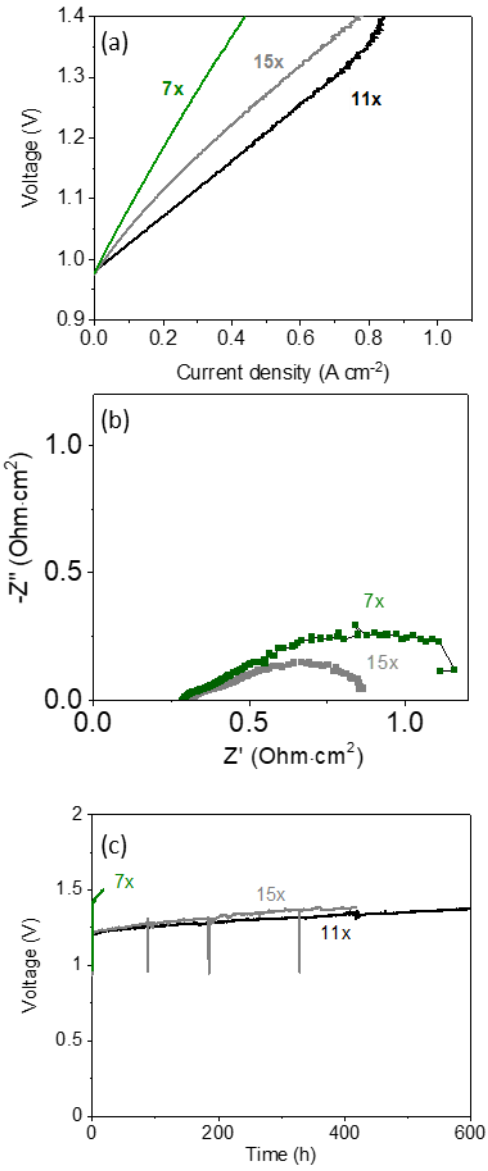

Figure 2. Oxygen catalyst infiltration cycles. (a) Initial performance (b) EIS and (c) durability of MS-SOFCs with varying infiltration cycles of LSCF-SDC oxygen electrodes and 11 infiltration cycles of SDCN steam electrodes at 700 °C and 50:50 H_2:H_2O. SEM images of varying infiltration cycles can be found in the supporting information.

Oxygen electrocatalysts are affected by the infiltration processing temperature. LSCF sintering typically occurs around 1100 °C or lower to minimize interdiffusion with adjacent materials. For MS-SOECs, an even lower processing temperature is required to avoid rapid oxidation of the metal support [8]. Infiltration temperature in the range between 650 and 900 °C is studied here. Powder XRD shows increased

perovskite peak intensity and narrower peak width ascribed to higher crystallinity with increasing temperature, Figure 3a. Higher crystallinity did not translate to higher performance. Higher treatment temperatures have been shown to reduce the apparent conductivity of LSCF. As treatment temperature has a significant impact on microstructure, agglomeration caused by higher temperatures reduces interconnectivity between LSCF particles thereby decreasing conductivity[26]. Also, there is a noticeable crystalline impurity phase at 850 °C and above. Performance and durability in the 750 to 850 °C range was superior to those at both lower and higher temperatures. Both high initial performance and low degradation are achieved at 800 °C, and this temperature was selected for further optimizations. Infiltrating at 800 °C may provide appropriate balance between LSCF crystallinity, secondary phase formation, particle contact and percolation, and Cr migration into the oxygen electrode. Cr is known to migrate from the metal support during infiltration, and the rate is expected to increase at higher processing temperature[14].

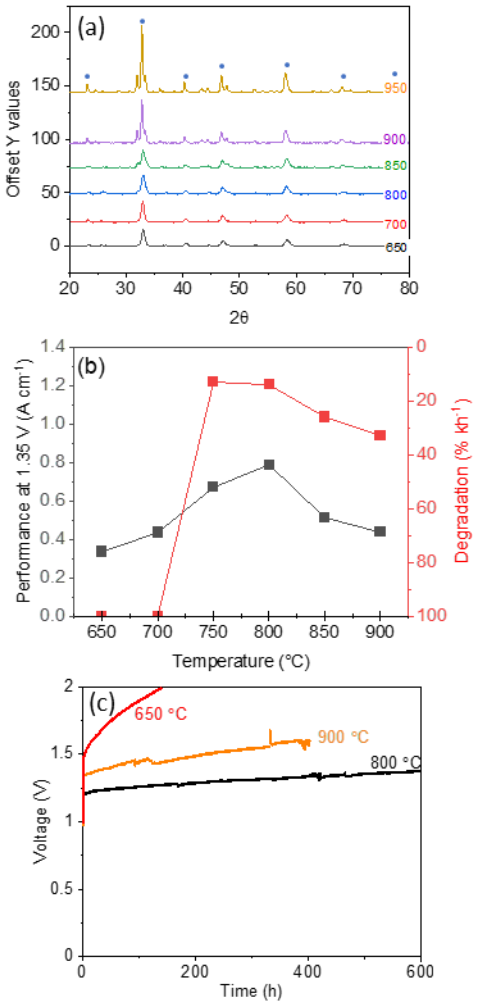

Figure 3. Oxygen catalyst infiltration temperature. (a) XRD spectra of LSCF precursor after calcining at varying temperatures (°C), with circles denoting LSCF phase peaks. (b) Initial performance and durability as a function of catalyst calcining temperature, and (c) durability at 700 °C operating temperature for cells with selected catalyst calcining temperatures.

Steam Electrode

Although Ni is the standard electrode for steam electrolysis, its long term durability at high temperature and in oxidizing environment is limited. Ni catalyst evolution is widely accepted to be a major cause of SOEC degradation [28]–[31]. Ni particle coarsening decreases the number of active sites, diminishing performance over time. In conventional electrodes, Ni migrates away from the electrolyte at temperatures below 900 °C resulting in loss of contact between Ni and zirconia particles. This is especially true at high current density such as 1 A cm^{-2} [32]. Curtailing current density to reduce degradation is

undesirable, however, as operating high-performance SOEC stacks around the thermo-neutral point requires high current density.

Ni:SDC ratio in the steam electrode of 40:60 vol% provides the best performance and durability, Figure 4. High Ni content leads to high performance, as Ni has higher electronic conductivity and electrocatalytic activity than SDC. SDCN40 and SDCN60 electrodes achieved initial performance above 0.8 A cm^{-2} at 1.35 V, Figure 4a. It is interesting that low Ni content (SDCN10) and even Ni-free SDC compositions provided moderate performance around 0.4 A cm^{-2} at 1.35 V, suggesting that pure SDC is a sufficient electrocatalyst for steam electrolysis. Ni coarsening was identified as a primary degradation mode for this MS-SOEC design[16]. Consistent with this previous finding, SDCN60 showed nearly twice the degradation rate of SDCN40 at 30% kh^{-1} and 14% kh^{-1}, respectively. Durability of the low Ni electrodes was similar to the SDCN40 electrode. Cells with no Ni degraded at a rate of 12 % kh^{-1} while SDCN10 electrodes degraded at 18 %kh^{-1}, suggesting that SDC evolution is a secondary degradation phenomenon. Based on these results, SDCN40 was selected as the best ratio. SEM imaging (found in the supporting information) was collected after operation. Images indicated that SDCN10 catalyst particles were < 50 nm in size, similar to fresh catalyst particle size after initial reduction, whereas SDCN60 particles coarsened significantly to 100 nm and larger. This reiterates that for higher Ni content, Ni coarsening is a primary degradation mode while SDC coarsening is a minor or secondary degradation mode.

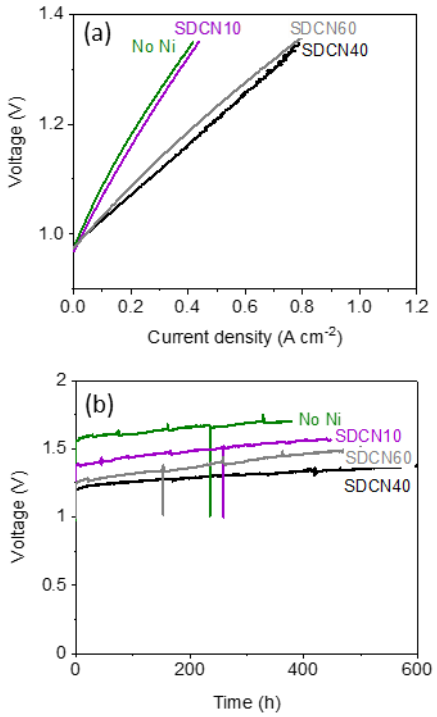

Figure 4. **Steam electrode catalysts.** (a) Initial performance and (b) durability of various steam electrodes for MS-SOECs at 700 °C and 50:50 H_2:H_2O. Oxygen electrocatalyst is LSCF-SDC for all cells.

Operating Temperature

Operating temperature significantly impacts the cell performance, Figure 5. MS-SOECs operating around 600 °C risk accelerating breakaway oxidation, as the Cr diffusion rate is lower than the Cr oxidation consumption rate at this temperature [8]. At operating temperatures of 650 °C and above, a normal protective Cr-based oxide scale is formed. Higher operating temperatures, however, can lead to increased particle agglomeration and pose a greater challenge in the choice of hermetic seals. Optimized cells with LSCF-SDC oxygen electrodes and SDCN40 steam electrodes with 11 infiltration cycles fired at 800 °C were operated in the range 650 to 750 °C. Initial performance exceeded 1A cm^{-2} at 1.3 V at 750 °C, Figure 5a. Initial performance at 700 °C and 650 °C was 0.8 A cm^{-2} and 0.45 A cm^{-2}, respectively. Stable long-term durability was observed at 700 °C. Faster degradation was observed at 750 °C; Ni agglomeration and Cr migration are both thermally activated. Due to low initial performance, 650 °C durability data was collected at 0.33 A cm^{-2} rather than 0.5 A cm^{-2}. Cell degradation remained low and stable at 650 °C for 300

h, and then started to increase. Thus, a relatively narrow operating temperature range around 700 °C is considered important to balance performance and durability. This may not be a problematic limitation, as SOECs operating around the thermoneutral voltage do not experience large temperature gradients[33].

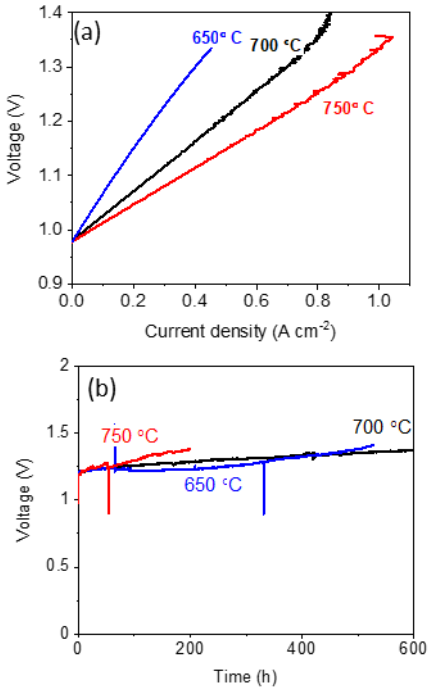

Figure 5. Operating temperature. (a) Initial performance and (b) durability of optimized MS-SOECs with 50:50 H_2:H_2O.

Cell Support Structure

The pore structure of the metal support can limit steam mass transport, similar to the oxygen mass transport restriction observed in SOFC mode[34]. Standard metal supports are approximately 250 µm thick. These give rise to a significant mass transport limitation at low steam content, leading to limiting current behavior, Figure 6. To improve mass transport, the metal support structure was made thinner (approximately 200 µm) and more porous (50% more poreformer added). Details of the metal support optimization is reported in reference [35]. When operating with 10% H_2O, the improved MS-SOEC had a limiting current of 0.250 A cm^{-2} compared to 0.175 A cm^{-2} for a standard cell. For 25% H_2O, the improved and standard cells had a limiting current of 0.430 and 0.288 A cm^{-2}, respectively. No limiting current was

apparent for either cell with 50% H_2O. Limiting currents were used to calculate the steam transport resistances using the methodology in Ref [36].Transport resistance at 25% steam was 209 sec m^{-1} for standard supports and 140 sec m^{-1} for thinner, more porous supports, resulting in improved limiting current performance for the latter. The improvement in limiting current would be valuable for a SOEC system operating at high H_2 recycle rate or high steam utilization.

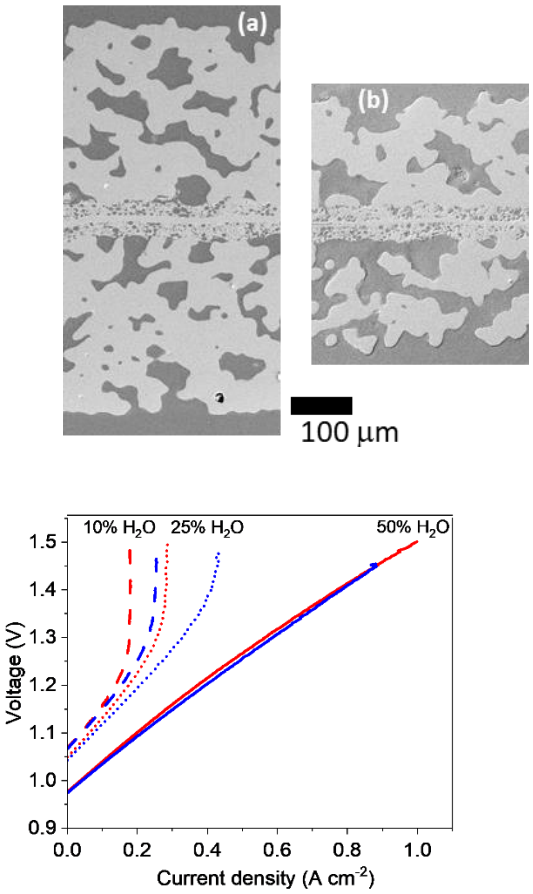

Figure 6. Impact of metal support structure on limiting current. SEM images of cells with (a) standard and (b) thinner, higher porosity metal support structures and (c) comparison of limiting current in these cells at various H_2O:H_2 ratios.

Conclusion

MS-SOECs were optimized for various parameters that influence performance and durability. Changing the oxygen catalyst composition produced little difference in degradation rate. A catalyst

composite of LSCF and SDC showed the best performance. The processing temperature of the oxygen catalyst had a significant impact, with 800 °C providing both the best performance and durability. Steam electrodes were optimized by varying the Ni content in the Ni-SDC catalyst mixture. While higher Ni content increased performance, higher degradation rates were also observed likely due to enhanced Ni particle coarsening. Removing or limiting Ni to 10 vol% significantly reduced performance, but durability remained comparable to cells with the optimum 40 vol% Ni content. Operating temperature was also found to affect long term durability of the optimized cells. The ideal operation temperature for these MS-SOECs is 700 °C, as this provides a suitable trade-off between performance and durability. Finally, steam mass transport limitation in the metal support was explored at low steam contents. Thinner and more-porous metal supports increase the limiting current compared to standard cells, at steam levels below 50%. This work demonstrates the necessity of tuning metal supported cells for electrolysis mode, as processing, composition, structure, and operational changes have profound effects on performance and durability. Continued MS-SOEC development is anticipated to allow performance to approach that of conventional ceramic cells. In turn, MS-SOECs can be used in dynamic applications where ceramic cells are limited and metal supports provide benefit.

Acknowledgements

The authors gratefully acknowledge research support from the HydroGEN Advanced Water Splitting Materials Consortium, established as part of the Energy Materials Network under the U.S. Department of Energy, Office of Energy Efficiency and Renewable Energy, Fuel Cell Technologies Office, under Contract Number DE-AC02-05CH11231. Fengyu Shen is thanked for assistance with SEM imaging. The use of Zeiss Gemini Ultra-55 FESEM in the Molecular Foundry of Lawrence Berkeley National Laboratory was supported by the Office of Science, Office of Basic Energy Sciences, of the U.S. Department of Energy under Contract No. DE-AC02-05CH11231. The views and opinions of the authors expressed herein do not necessarily state or reflect those of the United States Government or any agency thereof. Neither the United States Government nor any agency thereof, nor any of their employees, makes any warranty, expressed or

implied, or assumes any legal liability or responsibility for the accuracy, completeness, or usefulness of any information, apparatus, product, or process disclosed, or represents that its use would not infringe privately owned rights.

References

[1] I. Staffell *et al.*, "The role of hydrogen and fuel cells in the global energy system," *Energy Environ. Sci.*, vol. 12, no. 2, pp. 463–491, 2019, doi: 10.1039/C8EE01157E.

[2] S. D. Ebbesen, S. H. Jensen, A. Hauch, and M. B. Mogensen, "High Temperature Electrolysis in Alkaline Cells, Solid Proton Conducting Cells, and Solid Oxide Cells," *Chem. Rev.*, vol. 114, no. 21, pp. 10697–10734, Nov. 2014, doi: 10.1021/cr5000865.

[3] M. A. Laguna-Bercero, "Recent advances in high temperature electrolysis using solid oxide fuel cells: A review," *J. Power Sources*, vol. 203, pp. 4–16, Apr. 2012, doi: 10.1016/j.jpowsour.2011.12.019.

[4] M. Ni, M. K. H. Leung, and D. Y. C. Leung, "Technological development of hydrogen production by solid oxide electrolyzer cell (SOEC)," *Int. J. Hydrog. Energy*, vol. 33, no. 9, pp. 2337–2354, May 2008, doi: 10.1016/j.ijhydene.2008.02.048.

[5] A. Nechache, M. Cassir, and A. Ringuedé, "Solid oxide electrolysis cell analysis by means of electrochemical impedance spectroscopy: A review," *J. Power Sources*, vol. 258, pp. 164–181, Jul. 2014, doi: 10.1016/j.jpowsour.2014.01.110.

[6] G. Kaur, A. P. Kulkarni, and S. Giddey, "CO2 reduction in a solid oxide electrolysis cell with a ceramic composite cathode: Effect of load and thermal cycling," *Int. J. Hydrog. Energy*, vol. 43, no. 48, pp. 21769–21776, Nov. 2018, doi: 10.1016/j.ijhydene.2018.10.014.

[7] J. E. O'Brien, C. M. Stoots, J. S. Herring, and P. A. Lessing, "Performance Characterization of Solid-Oxide Electrolysis Cells for Hydrogen Production," in *2nd International Conference on Fuel Cell Science, Engineering and Technology*, Rochester, New York, USA, Jan. 2004, pp. 219–228. doi: 10.1115/FUELCELL2004-2474.

[8] M. C. Tucker, "Progress in metal-supported solid oxide electrolysis cells: A review," *Int. J. Hydrog. Energy*, vol. 45, no. 46, pp. 24203–24218, Sep. 2020, doi: 10.1016/j.ijhydene.2020.06.300.

[9] A. Nechache, F. Han, R. Semerad, G. Schiller, and R. Costa, "Evaluation of Performance and Degradation Profiles of a Metal Supported Solid Oxide Fuel Cell under Electrolysis Operation," *ECS Trans.*, vol. 78, no. 1, p. 3039, May 2017, doi: 10.1149/07801.3039ecst.

[10] Y.-S. Yoo, M. Choi, S. Yang, H.-J. Jin, M.-A. Park, and E.-H. Kim, "Fabrication and Performance Evaluation of Solid Oxide Electrolysis Cell Integrated with Metal Interconnect by Joining Process," *ECS Meet. Abstr.*, vol. MA2015-03, no. 1, p. 53, Jul. 2015, doi: 10.1149/MA2015-03/1/53.

[11] A. Hagen, R. Caldogno, F. Capotondo, and X. Sun, "Metal Supported Electrolysis Cells," *Energies*, vol. 15, no. 6, Art. no. 6, Jan. 2022, doi: 10.3390/en15062045.

[12] A. Hauch *et al.*, "Recent advances in solid oxide cell technology for electrolysis," *Science*, vol. 370, no. 6513, p. eaba6118, Oct. 2020, doi: 10.1126/science.aba6118.

[13] M. B. Mogensen *et al.*, "Reversible solid-oxide cells for clean and sustainable energy," *Clean Energy*, vol. 3, no. 3, pp. 175–201, Nov. 2019, doi: 10.1093/ce/zkz023.

[14] F. Shen, M. Reisert, R. Wang, P. Singh, and M. C. Tucker, "Assessment of Protective Coatings for Metal-Supported Solid Oxide Electrolysis Cells," *ACS Appl. Energy Mater.*, Jul. 2022, doi: 10.1021/acsaem.2c00655.

[15] R. Wang, E. Dogdibegovic, G. Y. Lau, and M. C. Tucker, "Metal-Supported Solid Oxide Electrolysis Cell with Significantly Enhanced Catalysis," *Energy Technol.*, vol. 7, no. 5, p. 1801154, 2019, doi: 10.1002/ente.201801154.

[16] F. Shen, R. Wang, and M. C. Tucker, “Long term durability test and post mortem for metal-supported solid oxide electrolysis cells,” *J. Power Sources*, vol. 474, p. 228618, Oct. 2020, doi: 10.1016/j.jpowsour.2020.228618.
[17] F. Shen, M. M. Welander, and M. C. Tucker, “Metal-Supported Solid Oxide Electrolysis Cell Test Standard Operating Procedure,” *Front. Energy Res.*, vol. 10, 2022, Accessed: Apr. 28, 2022. [Online]. Available: https://www.frontiersin.org/article/10.3389/fenrg.2022.817981
[18] M. C. Tucker, “Durability of symmetric-structured metal-supported solid oxide fuel cells,” *J. Power Sources*, vol. 369, pp. 6–12, Nov. 2017, doi: 10.1016/j.jpowsour.2017.09.075.
[19] M. Reisert, V. Berova, A. Aphale, P. Singh, and M. C. Tucker, “Oxidation of porous stainless steel supports for metal-supported solid oxide fuel cells,” *Int. J. Hydrog. Energy*, vol. 45, no. 55, pp. 30882–30897, Nov. 2020, doi: 10.1016/j.ijhydene.2020.08.015.
[20] F. Shen, M. M. Welander, and M. C. Tucker, “Oxidation of porous stainless steel supports for metal-supported solid oxide electrolysis cells,” *Int. J. Hydrog. Energy*, Jan. 2023, doi: 10.1016/j.ijhydene.2022.11.235.
[21] Y. Wang, W. Li, L. Ma, W. Li, and X. Liu, “Degradation of solid oxide electrolysis cells: Phenomena, mechanisms, and emerging mitigation strategies—A review,” *J. Mater. Sci. Technol.*, vol. 55, pp. 35–55, Oct. 2020, doi: 10.1016/j.jmst.2019.07.026.
[22] W. Wang, L. Gan, J. P. Lemmon, F. Chen, J. T. S. Irvine, and K. Xie, “Enhanced carbon dioxide electrolysis at redox manipulated interfaces,” *Nat. Commun.*, vol. 10, no. 1, Art. no. 1, Apr. 2019, doi: 10.1038/s41467-019-09568-1.
[23] P. V. Hendriksen, M. Khoshkalam, X. Tong, Đ. Tripković, M. A. Faghihi-Sani, and M. Chen, “Improving Oxygen Electrodes by Infiltration and Surface Decoration,” *ECS Trans.*, vol. 91, no. 1, pp. 1413–1424, Jul. 2019, doi: 10.1149/09101.1413ecst.
[24] F. Mauvy, J.-C. Grenier, J. Vulliet, J.-M. Bassat, and A. Rougier, “Lanthanum nickelate as an efficient oxygen electrode for solid oxide electrolysis cell,” *Fuel Cells*, vol. 22, no. 1–2, pp. 48–56, 2022, doi: 10.1002/fuce.202200013.
[25] M. A. Laguna-Bercero, H. Monzón, A. Larrea, and V. M. Orera, “Improved stability of reversible solid oxide cells with a nickelate-based oxygen electrode,” *J. Mater. Chem. A*, vol. 4, no. 4, pp. 1446–1453, 2016, doi: 10.1039/C5TA08531D.
[26] J. Ju, Y. Xie, Z. Wang, Y. Zhang, and C. Xia, “Electrical Performance of Nano-Structured La0.6Sr0.4Co0.2Fe0.8O3-δ Impregnated onto Yttria-Stabilized Zirconia Backbone,” *J. Electrochem. Soc.*, vol. 163, no. 5, p. F393, Jan. 2016, doi: 10.1149/2.0751605jes.
[27] J. M. Vohs and R. J. Gorte, “High-Performance SOFC Cathodes Prepared by Infiltration,” *Adv. Mater.*, vol. 21, no. 9, pp. 943–956, 2009, doi: 10.1002/adma.200802428.
[28] D. Dogu, S. Gunduz, K. E. Meyer, D. J. Deka, A. C. Co, and U. S. Ozkan, “CO2 and H2O Electrolysis Using Solid Oxide Electrolyzer Cell (SOEC) with La and Cl- doped Strontium Titanate Cathode,” *Catal. Lett.*, vol. 149, no. 7, pp. 1743–1752, Jul. 2019, doi: 10.1007/s10562-019-02786-8.
[29] D. J. Deka *et al.*, “Hydrogen Production from Water in a Solid Oxide Electrolysis Cell: Effect of Ni Doping on Lanthanum Strontium Ferrite Perovskite Cathodes,” *Ind. Eng. Chem. Res.*, vol. 58, no. 50, pp. 22497–22505, Dec. 2019, doi: 10.1021/acs.iecr.9b03731.
[30] M. Chen *et al.*, “Microstructural Degradation of Ni/YSZ Electrodes in Solid Oxide Electrolysis Cells under High Current,” *J. Electrochem. Soc.*, vol. 160, no. 8, pp. F883–F891, 2013, doi: 10.1149/2.098308jes.
[31] A. Hagen and H. L. Frandsen, “Recent Highlights of Solid Oxide Fuel Cell and Electrolysis Research at DTU Energy,” *ECS Trans.*, vol. 103, no. 1, pp. 327–336, Jul. 2021, doi: 10.1149/10301.0327ecst.
[32] M. B. Mogensen *et al.*, “Review of Ni migration in SOC electrodes,” p. 10, 2020.
[33] J. Schefold, A. Brisse, A. Surrey, and C. Walter, “80,000 current on/off cycles in a one year long steam electrolysis test with a solid oxide cell,” *Int. J. Hydrog. Energy*, vol. 45, no. 8, pp. 5143–5154, Feb. 2020, doi: 10.1016/j.ijhydene.2019.05.124.

[34] E. Dogdibegovic, Y. Fukuyama, and M. C. Tucker, “Ethanol internal reforming in solid oxide fuel cells: A path toward high performance metal-supported cells for vehicular applications,” *J. Power Sources*, vol. 449, p. 227598, Feb. 2020, doi: 10.1016/j.jpowsour.2019.227598.
[35] B. Hu, G. Lau, D. Song, Y. Fukuyama, and M. C. Tucker, “Optimization of metal-supported solid oxide fuel cells with a focus on mass transport,” *J. Power Sources*, vol. 555, p. 232402, Jan. 2023, doi: 10.1016/j.jpowsour.2022.232402.
[36] Y. Fukuyama, T. Shiomi, T. Kotaka, and Y. Tabuchi, “The Impact of Platinum Reduction on Oxygen Transport in Proton Exchange Membrane Fuel Cells,” *Electrochimica Acta*, vol. 117, pp. 367–378, Jan. 2014, doi: 10.1016/j.electacta.2013.11.179.